**Supplementary Information**

# A next-generation dual-recombinase system for time- and host-specific targeting of pancreatic cancer

Nina Schönhuber, Barbara Seidler, Kathleen Schuck, Christian Veltkamp, Christina Schachtler, Magdalena Zukowska, Stefan Eser, Thorsten B. Feyerabend, Mariel C. Paul, Philipp Eser, Sabine Klein, Andrew M. Lowy, Ruby Banerjee, Fangtang Yang, Chang-Lung Lee, Everett J. Moding, David G. Kirsch, Angelika Scheideler, Dario R. Alessi, Ignacio Varela, Allan Bradley, Alexander Kind, Angelika E. Schnieke, Hans-Reimer Rodewald, Roland Rad, Roland M. Schmid, Günter Schneider and Dieter Saur

## Supplementary Figures

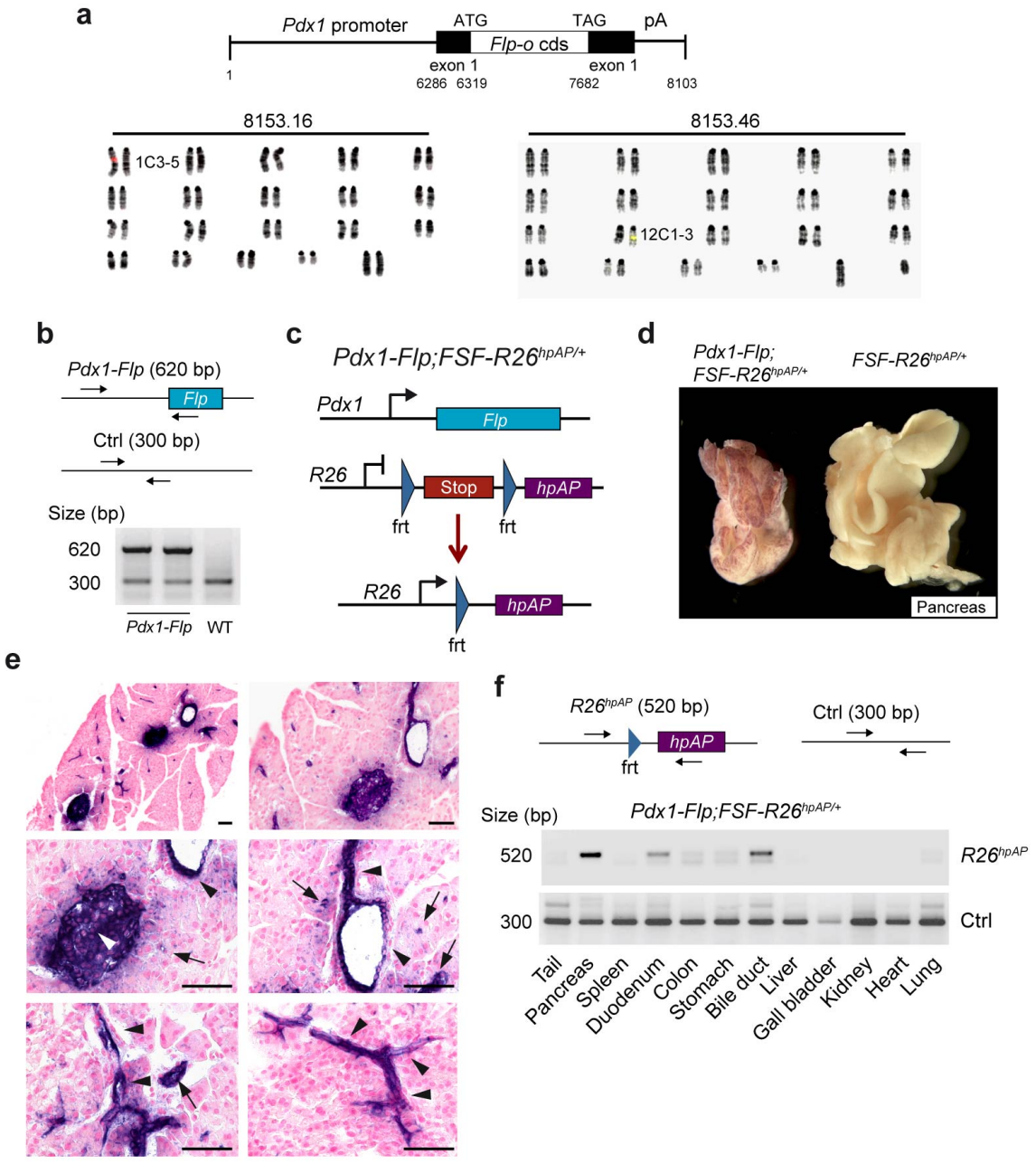


**Supplementary Figure 1** Flp-mediated recombination of the pancreas. (**a**) Upper panel: Scheme of the structure of the *Pdx1-Flp-o* transgene. The ATG of the *Flp-o* coding sequence is directly fused with the *Pdx1* ATG start codon. Lower panels: Fluorescence *in situ* hybridization (FISH) analysis shows integration of the transgene in chromosome 1 (C3-5; 8153.16 line) and chromosome 12 (C1-3; 8153.46 line). (**b**) Genotyping strategy of the *Pdx1-Flp-o* transgene (upper panel). PCR analysis of DNA from wild-type (WT) and transgenic *Pdx1-Flp* animals (lower panel). Sizes of WT and mutant PCR products are indicated. (**c**) Flp/frt recombination system based lineage tracing strategy for the transgenic *Pdx1-Flp* mouse lines with a *human placental alkaline phosphatase* (*hpAP*) reporter allele. (**d**) Alkaline phosphatase (AP) staining (purple color) of pancreatic whole mount tissue of 3 month-old male mice with indicated genotypes. (**e**) AP staining of pancreatic sections demonstrates *Pdx1-Flp*-mediated recombination of pancreatic islets (white arrow heads), ducts (black arrow heads) and acini (black arrows) in 3 month-old male animal. (**f**) PCR analyses of *Pdx1-Flp*-mediated deletion of the frt-stop-frt (FSF) cassette in the indicated tissues of a female *Pdx1-Flp;FSF-R26*$^{hpAP/+}$ mouse. Note: All results shown in b–f were obtained with the 8153.46 mouse line.

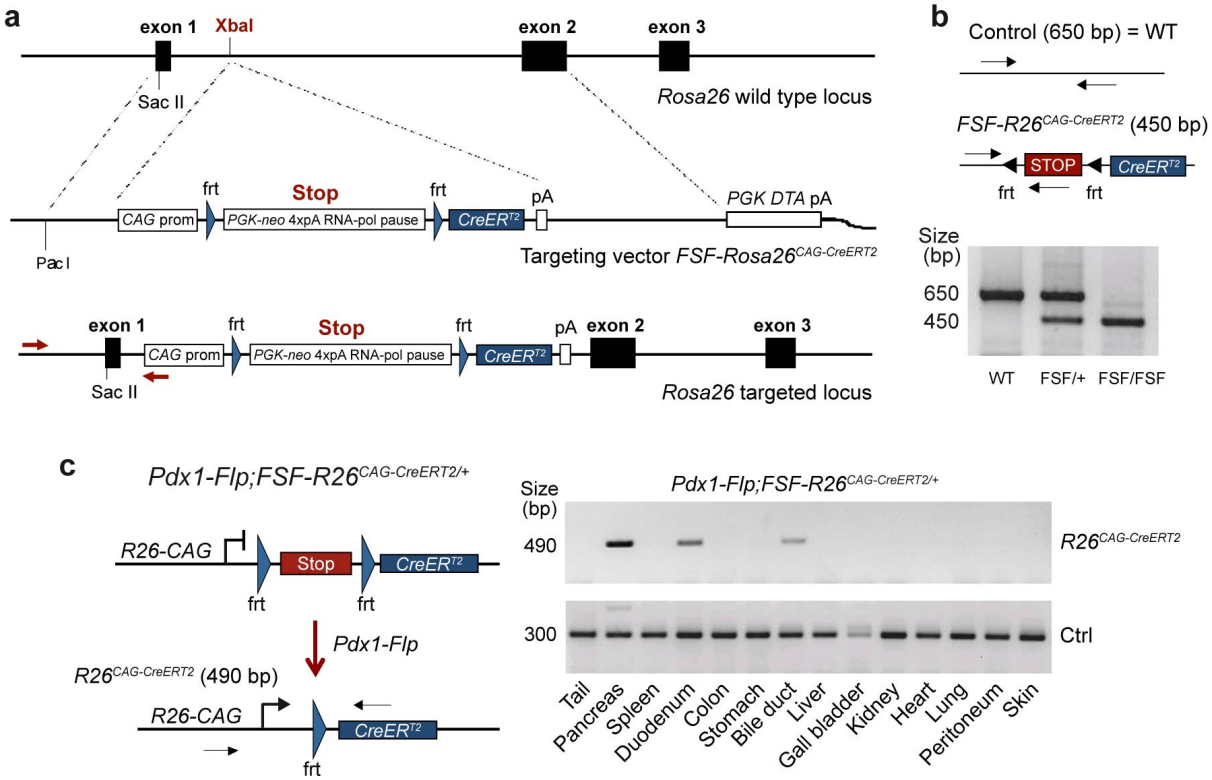
a
exon 1
XbaI
exon 2
exon 3
Sac II
Rosa26 wild type locus
frt
Stop
frt
pA
PGK DTA pA
CAG prom
PGK-neo 4xpA RNA-pol pause
CreER^T2
Pac I
Targeting vector FSF-Rosa26^CAG-CreERT2
exon 1
frt
Stop
frt
pA
exon 2
exon 3
CAG prom
PGK-neo 4xpA RNA-pol pause
CreER^T2
Sac II
Rosa26 targeted locus
b
Control (650 bp) = WT
FSF-R26^CAG-CreERT2 (450 bp)
STOP
CreER^T2
frt
frt
Size (bp)
650
450
WT
FSF/+
FSF/FSF
c
Pdx1-Flp;FSF-R26^CAG-CreERT2/+
R26-CAG
Stop
CreER^T2
frt
frt
Pdx1-Flp
R26^CAG-CreERT2 (490 bp)
R26-CAG
CreER^T2
frt
Pdx1-Flp;FSF-R26^CAG-CreERT2/+
Size (bp)
490
300
R26^CAG-CreERT2
Ctrl
Tail
Pancreas
Spleen
Duodenum
Colon
Stomach
Bile duct
Liver
Gall bladder
Kidney
Heart
Lung
Peritoneum
Skin
d
Pdx1-Flp;FSF-R26^CAG-CreERT2;R26^mT-mG
R26-CAG
tomato
pA
EGFP
loxP
loxP
CreER^T2
+ TAM
R26-CAG
EGFP
loxP
– TAM
– TAM
– TAM
+ TAM
+ TAM
+ TAM
tdTomato/EGFP/TOPRO
e
Amylase
Insulin
CK19
EGFP
Amylase
tdTomato
EGFP
Insulin
tdTomato
EGFP
CK19
tdTomato
+ TAM

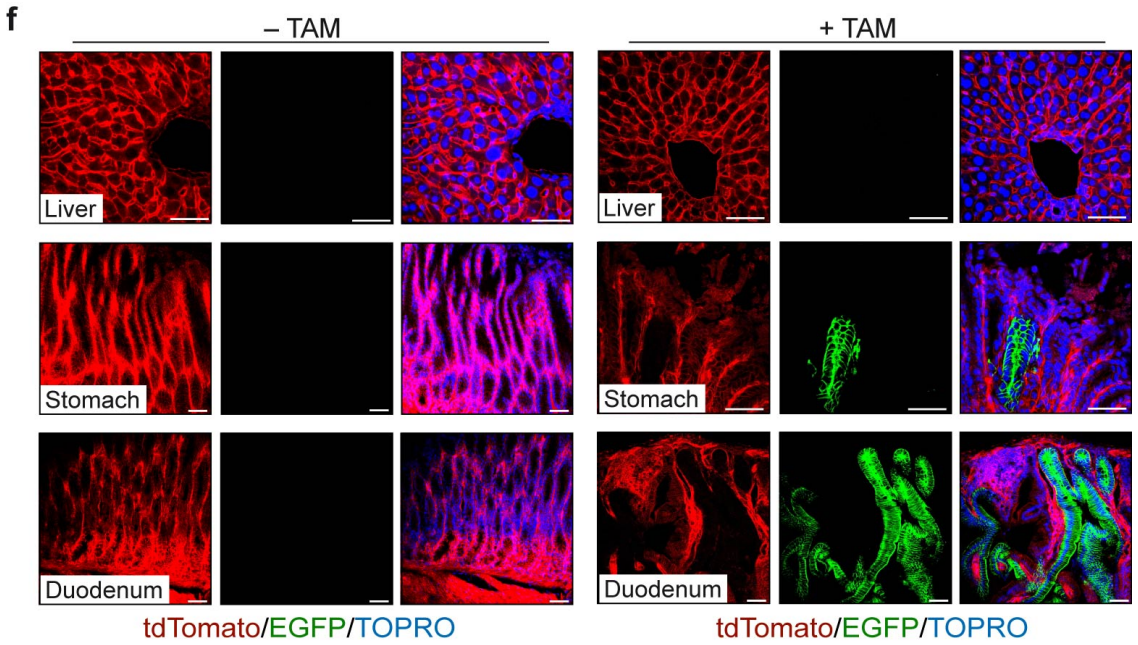


**Supplementary Figure 2** Sequential targeting of pancreas epithelium using a dual-recombination strategy. (**a**) *Rosa26* targeting. From top to bottom, diagrams of: *Rosa26* wild-type locus; the *Rosa26* targeting vector with the frt-stop-frt (FSF) silenced *CreER*$^{T2}$ expression cassette and the *CAG* promoter; the targeted *Rosa26* locus. Restriction sites and the exon structure of the *R26* locus are indicated. (**b**) Genotyping strategy of *FSF-R26*$^{CAG\text{-}CreERT2}$ mice (upper panel). PCR analysis of DNA from wild-type (WT), heterozygous (FSF/+) and homozygous (FSF/FSF) *FSF-R26*$^{CAG\text{-}CreERT2}$ mice (lower panel). Sizes of WT and mutant PCR products are indicated. (**c**) Genetic strategy used to activate CreER$^{T2}$ expression under control of the *CAG* promoter from the *Rosa26* locus (left panel) by Flp recombinase expression. PCR analyses of *Pdx1-Flp* induced deletion of the FSF cassette in the *Rosa26* locus of 3 month-old female *Pdx1-Flp;FSF-R26*$^{CAG\text{-}CreERT2/+}$ mice in indicated tissues (right panel). (**d**) Genetic tracing strategy used to monitor tamoxifen-mediated CreER$^{T2}$ activation in the Flp-lineage. A double-fluorescent floxed tdTomato-EGFP reporter line (*R26*$^{mT\text{-}mG}$) is used in which Cre induces a switch from membrane tagged tdTomato to membrane tagged EGFP expression (left panel). Representative confocal microscopic images of the pancreas of tamoxifen (+ TAM) and vehicle (– TAM) treated *Pdx1-Flp;FSF-R26*$^{CAG\text{-}CreERT2}$*;R26*$^{mT\text{-}mG}$ compound mutant female mice (right panel). Activation of CreER$^{T2}$ by tamoxifen induces EGFP expression (green) in pancreas epithelium. Red color shows expression of tdTomato in cells without Cre-mediated recombination. Nuclei were counterstained with TOPRO-3 (blue). (**e**) Immunofluorescence staining (red color) of acini (α-amylase; upper panel), islets (insulin; middle panel) and ducts (CK19, lower panel) of TAM-treated male *Pdx1-Flp;FSF-R26*$^{CAG\text{-}CreERT2}$*;R26*$^{mT\text{-}mG}$ animals. Note: Blue color shows expression of tdTomato in unrecombined cells. Green color labels Cre-recombined cells that express EGFP. (**f**) Representative confocal microscopic images of indicated tissues of tamoxifen (+ TAM) and vehicle (– TAM) treated *Pdx1-Flp;FSF-R26*$^{CAG\text{-}CreERT2}$*;R26*$^{mT\text{-}mG}$ compound mutant male and female mice. Activation of CreER$^{T2}$ by tamoxifen induces membrane tagged EGFP expression (green). Red color shows expression of membrane tagged tdTomato in cells without Cre induced recombination. Nuclei were counterstained with TOPRO-3 (blue). Scale bars, 50 μm.

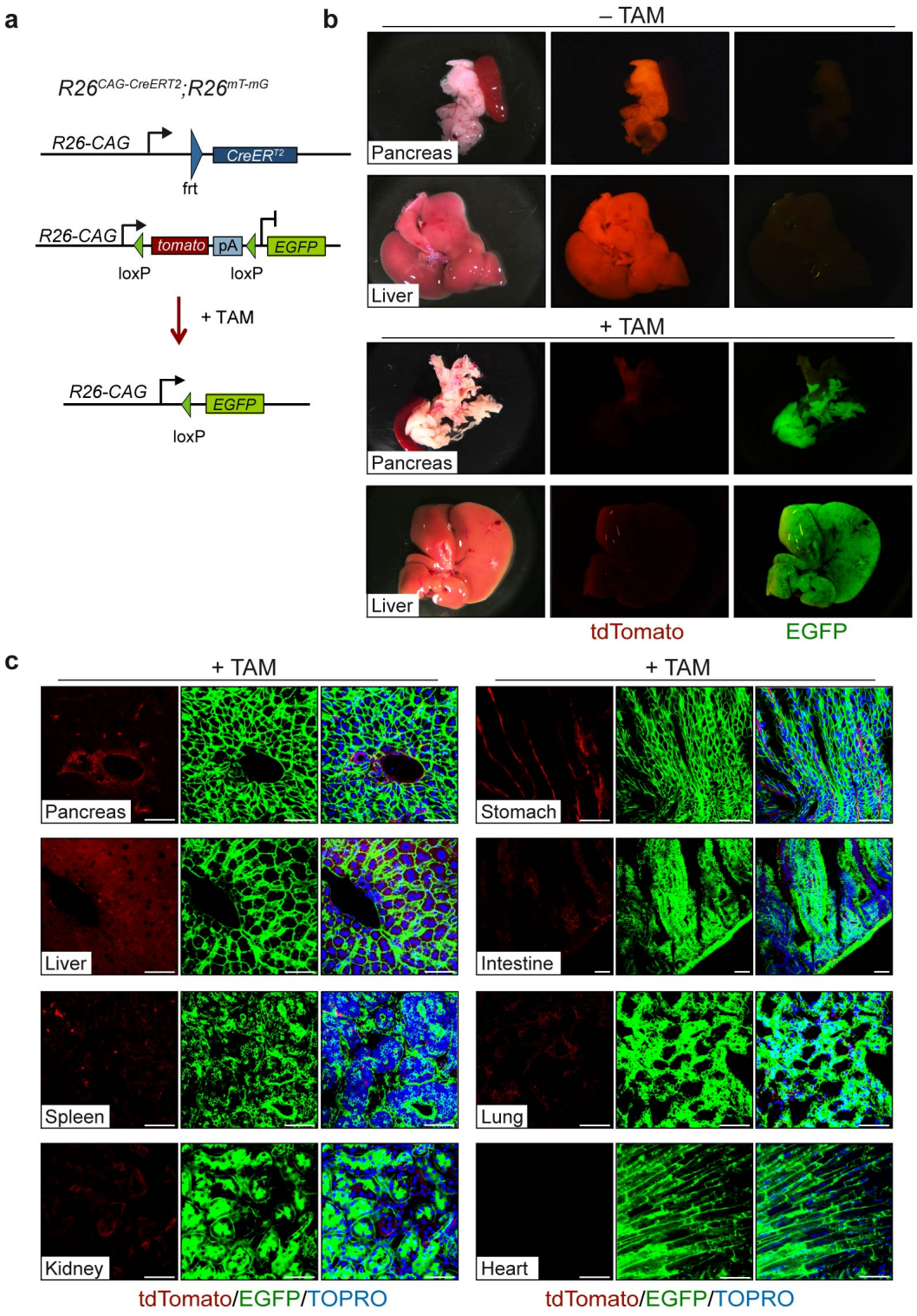


**Supplementary Figure 3** Inducible Cre-mediated gene targeting in the whole organism. (**a**) Genetic strategy to monitor tamoxifen-mediated CreER$^{T2}$ activation and EGFP expression in the whole body by using the *R26*$^{CAG\text{-}CreERT2}$ deleter mouse line. (**b**) Macroscopic view of the pancreas and liver of tamoxifen (+ TAM) and vehicle (– TAM) treated male and female animals. White-light (left panel) and corresponding fluorescent images are shown. tdTomato (red color; non Cre-recombined cells; middle panel) and EGFP (green color; Cre-recombined cells; right panel) expression was visualized by fluorescence stereomicroscopy. (**c**) Representative confocal microscopic images of tdTomato (red color, non Cre-recombined cells) and Cre-induced EGFP (green color) expression in indicated tissues of tamoxifen-treated male animals. Nuclei were counterstained with TOPRO-3 (blue). Scale bars, 50 µm.

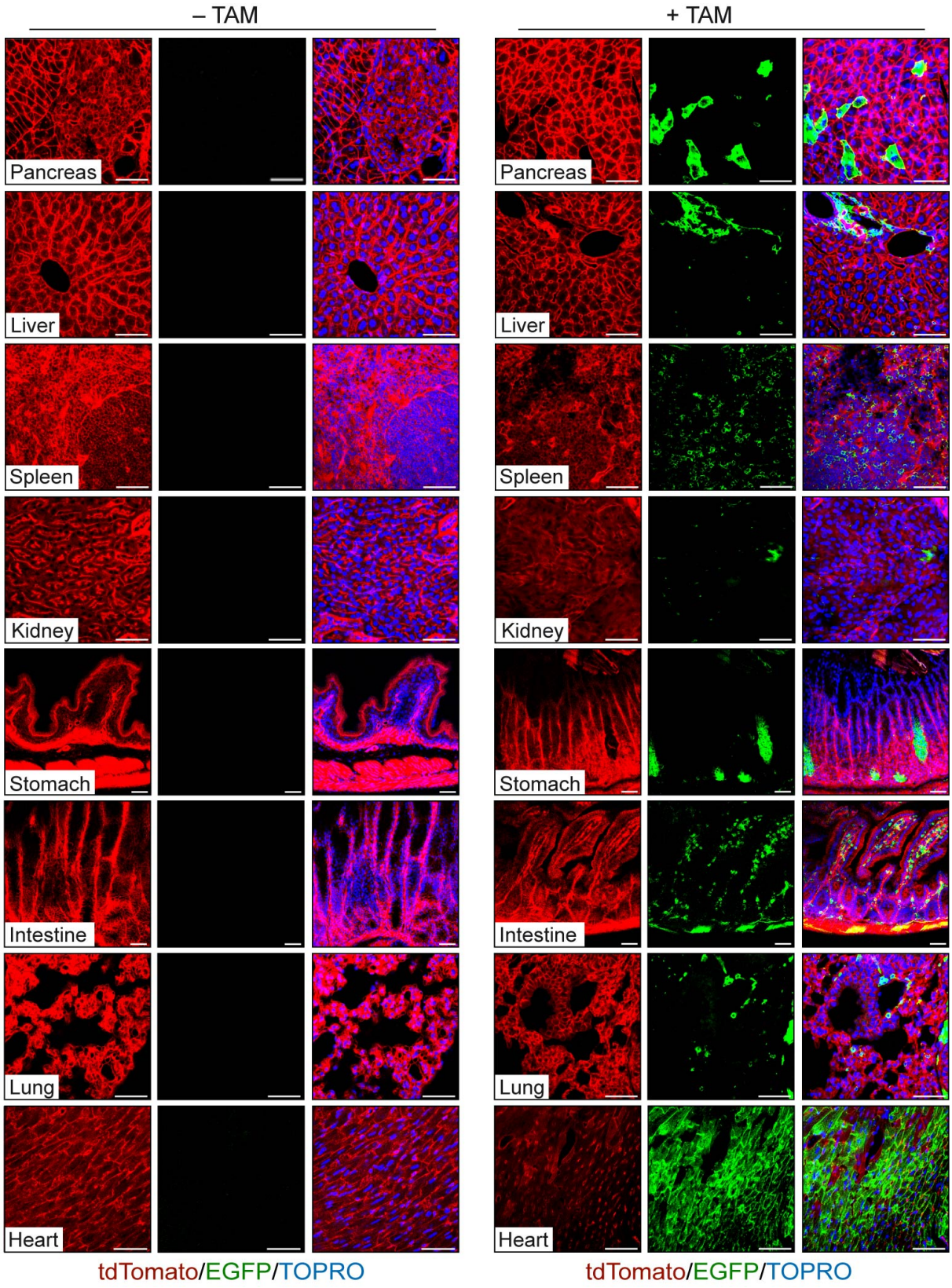


**Supplementary Figure 4** Sporadic Cre-mediated gene targeting in the whole body by low-dose tamoxifen treatment. Representative confocal microscopic images of low-dose tamoxifen-treated (+ TAM) and vehicle-treated (– TAM) *R26*$^{CAG\text{-}CreERT2}$;*R26*$^{mT\text{-}mG}$ female mice. tdTomato expression is shown in red color (non Cre-recombined cells) and Cre-induced EGFP expression is shown in green color in indicated tissues. Nuclei were counterstained with TOPRO-3 (blue). Scale bars, 50 µm.

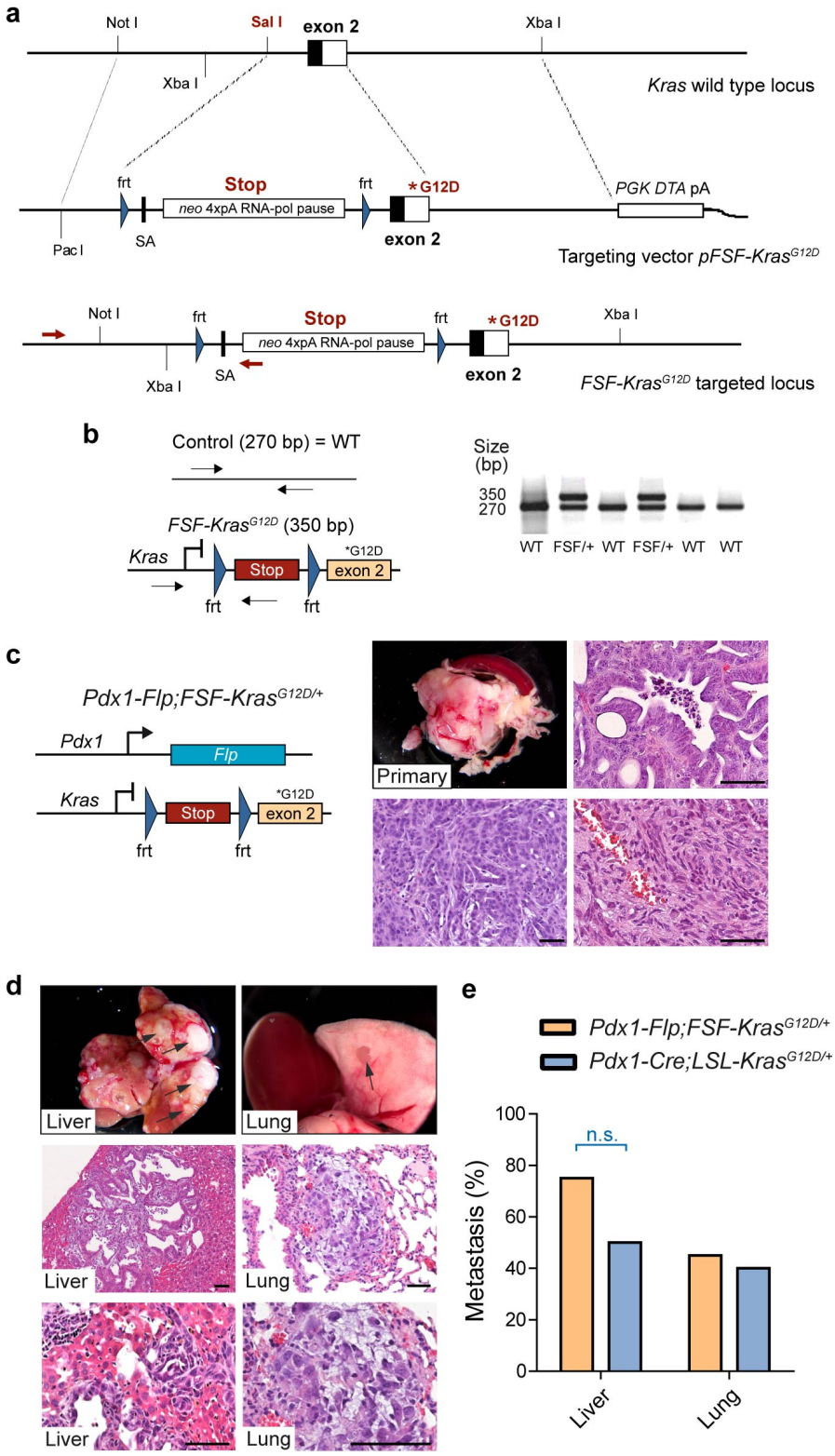


**Supplementary Figure 5** *Pdx1-Flp*-mediated activation of oncogenic Kras$^{G12D}$ in pancreas induces metastatic PDAC. (**a**) Targeting the endogenous *Kras* locus. From top to bottom, diagrams of: *Kras* wild-type locus; the *pFSF-Kras$^{G12D}$* targeting vector with the promoterless frt-stop-frt (FSF) gene trapping cassette 5′ of Kras exon 2 which contains the oncogenic codon 12 (G12D) mutation; the targeted *FSF-Kras$^{G12D}$* locus. Restriction sites and the exon structure of the *Kras* locus are indicated. SA, splice acceptor. (**b**) Genotyping strategy of *FSF-Kras$^{G12D}$* mice (left panel). PCR analysis of DNA from wild-type (WT) and heterozygous (FSF/+) *FSF-Kras$^{G12D/+}$* mice (right panel). Sizes of WT and mutant PCR products are indicated. (**c**) Representative

macroscopic view of primary PDAC and microscopic images of H&E stained PDAC tissue sections of *Pdx1-Flp;FSF-Kras*$^{G12D/+}$ male and female mice. (**d**) Representative macroscopic view (upper panel) and microscopic H&E stained tissue sections (lower panels) of PDAC associated liver and lung metastasis (indicated by black arrows in the upper panel) in male and female *Pdx1-Flp;FSF-Kras*$^{G12D/+}$ (KF) mice. (**e**) Incidence of metastasis in male and female KF and *Pdx1-Cre;LSL-Kras*$^{G12D/+}$ (KC) mice. Bar graph shows the percentage of mice with liver and lung metastases detected by macroscopic and microscopic histopathological analysis (*n* = 20 mice per genotype; n.s., not significant by Fisher's exact test). Scale bars, 50 μm.

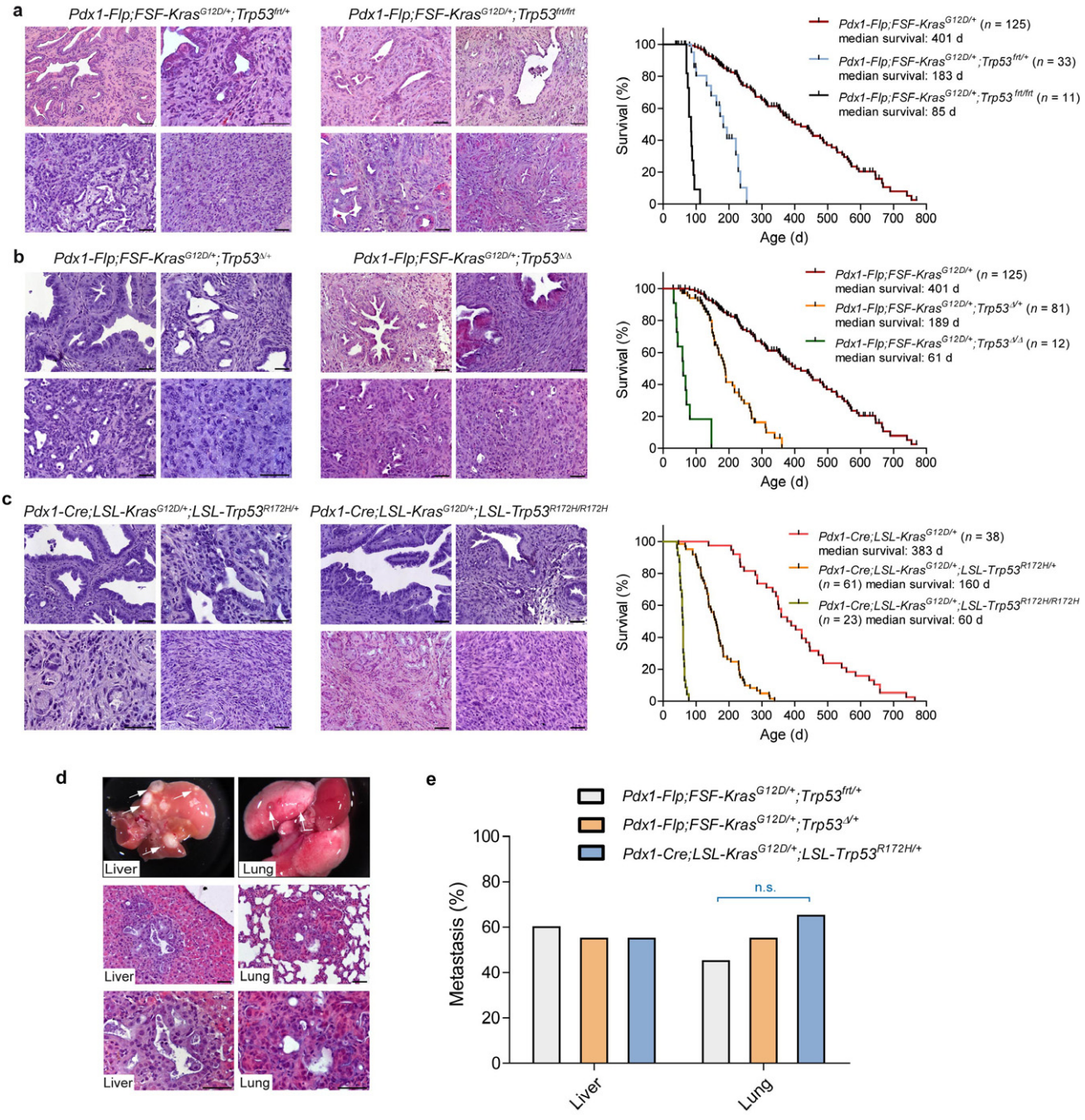


**Supplementary Figure 6** Inactivation of the tumor suppressor p53 accelerates PDAC formation. (**a**) Representative H&E stained tissue section of well-to-moderately differentiated (upper panel) and undifferentiated (lower panel) PDAC from male and female mice of the KPF model (*Pdx1-Flp;FSF-Kras*$^{G12D/+}$*;Trp53*$^{frt}$). Mice carry a heterozygous (left panel) or homozygous (middle panel) frt-flanked *p53* allele. Right panel: Kaplan-Meier survival curves of the indicated genotypes. '$^{+}$' denotes the wild type allele, '*p53*$^{frt}$' denotes the conditional frt flanked *Trp53* allele. (**b**) Representative H&E stained tissue section of well-to-moderately differentiated (upper panel) and undifferentiated (lower panel) PDAC from male and female mice with a heterozygous (left panel) or homozygous (right panel) deletion of *p53* in the whole body (*Pdx1-Flp;FSF-Kras*$^{G12D/+}$*;Trp53*$^{\Delta}$). Right panel: Kaplan-Meier survival curves of the indicated genotypes. '$^{+}$' denotes the wild type allele, '*p53*$^{\Delta}$' denotes the constitutively deleted *Trp53* allele in the whole animal. (**c**) Representative H&E stained tissue section of well-to-moderately differentiated (upper panel) and undifferentiated (lower panel) PDAC from male and female mice of the established Cre/loxP based KPC model (*Pdx1-Cre;LSL-Kras*$^{G12D/+}$*;LSL-Trp53*$^{R172H}$). Mice express mutant p53$^{R172H}$

heterozygous (left panel) or homozygous (middle panel) in the pancreas. Right panel: Kaplan-Meier survival curves of the indicated genotypes. '$^{+}$' denotes the wild type allele, '*LSL-Trp53*$^{R172H}$, denotes the conditional mutant *p53* allele. Expression of mutant Trp53$^{R172H}$ is blocked by a floxed stop cassette (LSL) in this model, resulting in a whole body *p53* knock-out in homozygous animals. (**d**) Representative macroscopic view (upper panel) and microscopic H&E stained tissue sections (lower panels) of PDAC associated liver and lung metastasis (indicated by white arrows in the upper panel) in *Pdx1-Flp;FSF-Kras*$^{G12D/+}$*;Trp53*$^{frt/+}$ (KPF) male and female mice. (**e**) Quantification of PDAC male and female mice with microscopic liver or lung metastasis of indicated genotypes (*n* = 20 mice per genotype). Bar graph shows the percentage of PDAC mice with microscopic liver and lung metastases (n.s., not significant by Fisher's exact test). Scale bars, 50 μm.

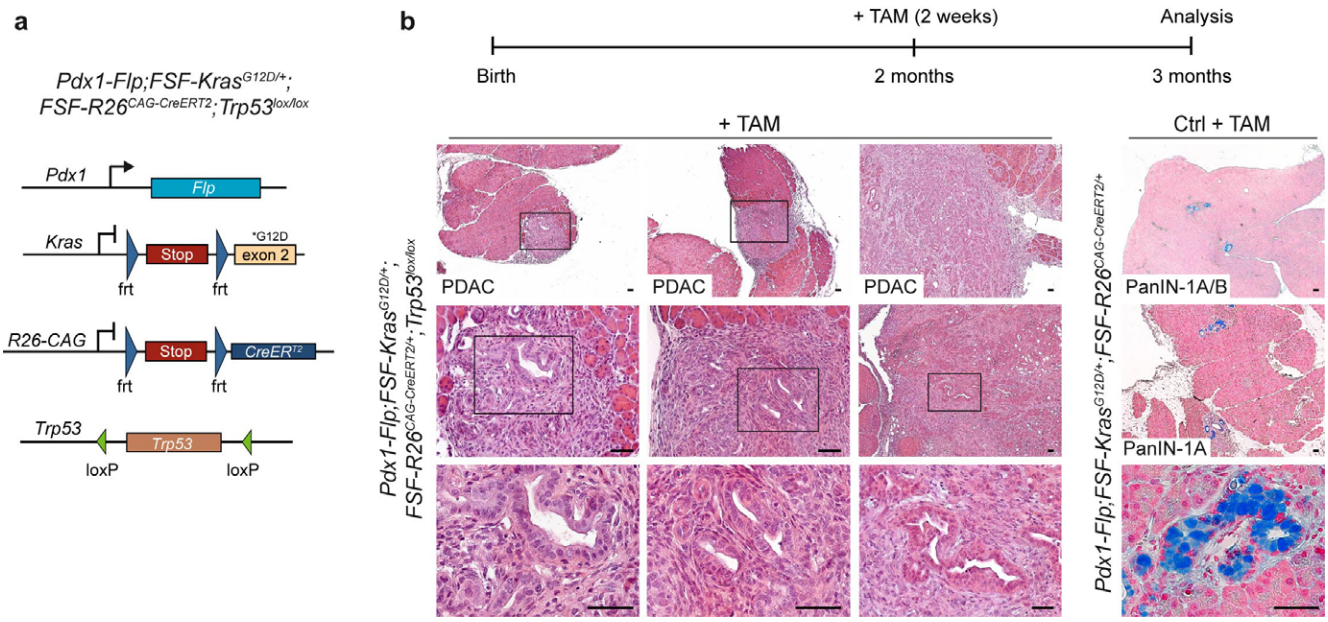


**Supplementary Figure 7** Modeling of multistep carcinogenesis by time specific p53 inactivation. (**a**) Genetic strategy used to inactivate p53 in the Flp-lineage by tamoxifen-mediated CreER$^{T2}$ activation. (**b**) Upper panel: Schematic of tamoxifen (TAM) treatment protocol. Lower panel: Representative alcian blue (blue color) and H&E stained pancreatic sections of TAM-treated *Pdx1-Flp;FSF-Kras$^{G12D/+}$;FSF-R26$^{CAG\text{-}CreERT2/+}$;Trp53$^{lox/lox}$* mice (left panel) and TAM-treated *Pdx1-Flp;FSF-Kras$^{G12D/+}$;FSF-R26$^{CAG\text{-}CreERT2/+}$* age- and sex-matched male and female controls without floxed *p53* alleles (right panel). Note: Multifocal PDAC development in all floxed *p53$^{lox/lox}$* animals (*n* = 3), but not in Ctrl animals without the floxed *p53* allele (*n* = 3). Scale bars, 50 µm.

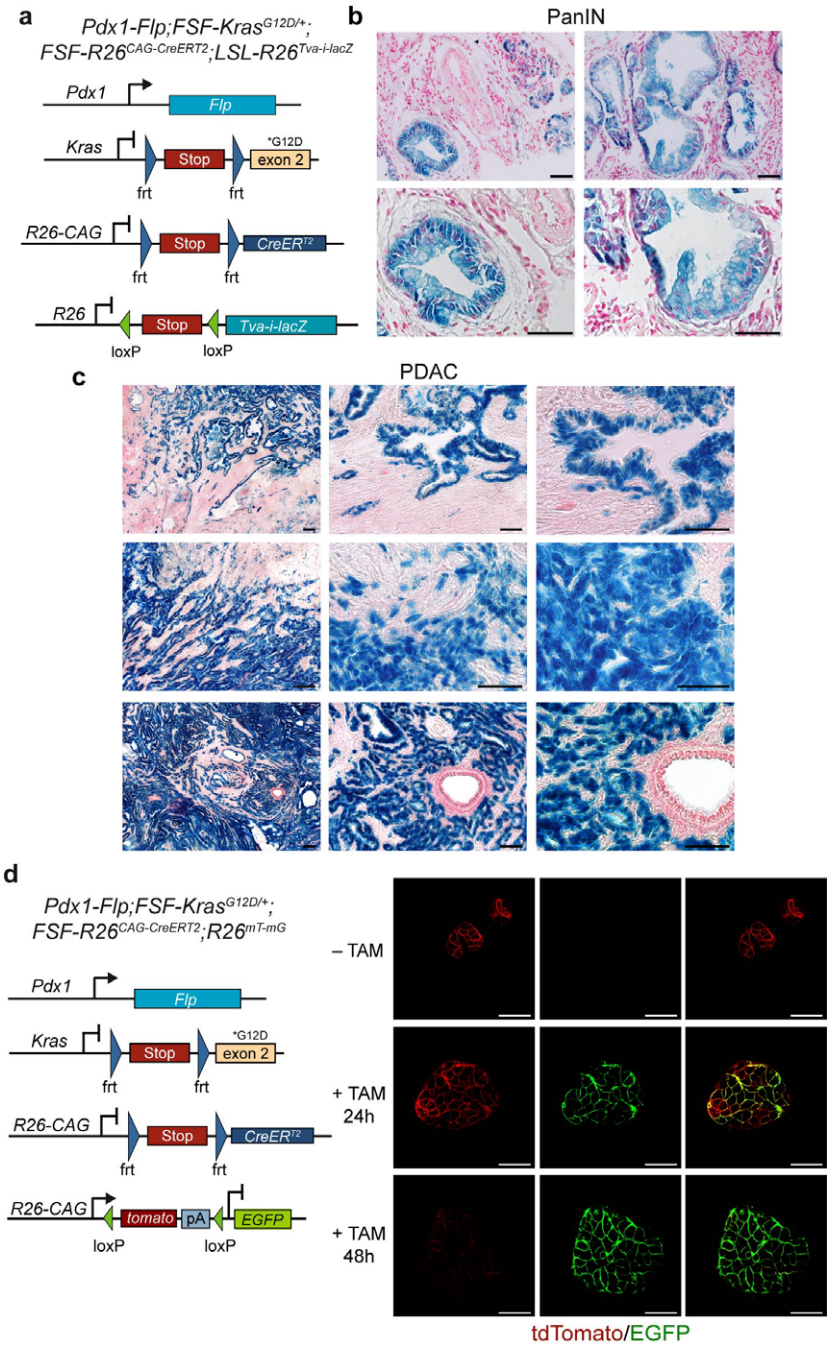


**Supplementary Figure 8** Secondary genetic manipulation of Kras$^{G12D}$-induced PanIN lesions and PDAC in the *Pdx1-Flp* lineage. (**a**) Genetic strategy used to induce lacZ expression in the Flp-lineage by tamoxifen-mediated CreER$^{T2}$ activation. (**b**) Representative β-galactosidase staining shows expression of lacZ in PanIN lesions but not desmoplastic stroma of tamoxifen-treated female *Pdx1-Flp;FSF-Kras$^{G12D/+}$;FSF-R26$^{CAG-CreERT2}$;LSL-R26$^{Tva-i-lacZ}$* mice. (**c**) Representative β-galactosidase staining shows expression of lacZ in stroma-rich well-differentiated (upper panel), undifferentiated sarcomatoid (middle panel) and mixed-differentiated (lower panel) PDAC tumors, but not desmoplastic stroma of tamoxifen-treated male *Pdx1-Flp;FSF-Kras$^{G12D/+}$;FSF-R26$^{CAG-CreERT2}$;LSL-R26$^{Tva-i-lacZ}$* mice. (**d**) Genetic strategy to induce EGFP expression by tamoxifen-mediated CreER$^{T2}$ activation (left panel). PDAC cells isolated from a female *Pdx1-Flp;FSF-Kras$^{G12D/+}$;FSF-R26$^{CAG-CreERT2}$;R26$^{mT-mG}$* mouse, which has not been treated with tamoxifen, were incubated with 0.1 μM 4-hydroxytamoxifen (TAM) *in vitro*. tdTomato (red color, non Cre-recombined cells) and Cre-induced EGFP (green color) expression was analyzed by confocal laser scanning microscopy at indicated time points (right panel). Scale bars, 50 μm.

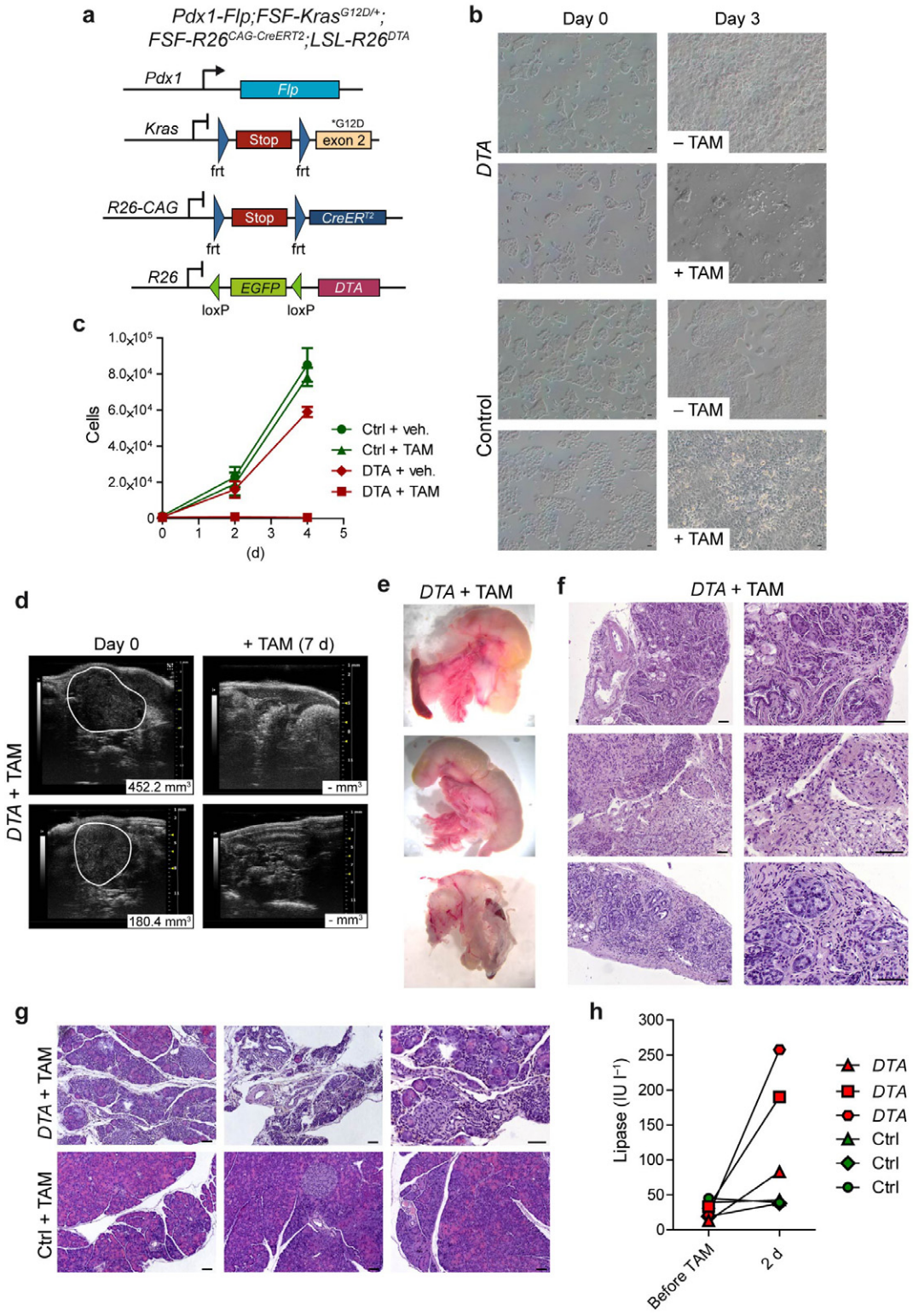


**Supplementary Figure 9** Secondary Cre-mediated DTA expression in established PDAC induces tumor regression *in vitro and in vivo*. (**a**) Genetic strategy used to induce diphtheria toxin A (DTA) expression in established PDAC by tamoxifen-mediated CreER$^{T2}$ activation. (**b**) PDAC cells isolated from tamoxifen naïve male *Pdx1-Flp;FSF-Kras$^{G12D/+}$;FSF-R26$^{CAG-CreERT2}$;LSL-R26$^{DTA}$* (*DTA*) and *Pdx1-Flp;FSF-Kras$^{G12D/+}$;FSF-R26$^{CAG-CreERT2/+}$* (control) mouse, were incubated with 0.5 µM 4-hydroxytamoxifen (+ TAM) or vehicle (– TAM) *in vitro*. Representative microscopic white light images of PDAC cells before and after 3 d of tamoxifen treatment are shown. (**c**) Proliferation of 4-hydroxytamoxifen (+ TAM) and vehicle (veh.) treated *DTA* and control (Ctrl)

cells monitored over time by cell counting (mean, ± s.e.m.). (**d**) Tumor growth in *Pdx1-Flp;FSF-Kras$^{G12D/+}$;FSF-R26$^{CAG\text{-}CreERT2}$;LSL-R26$^{DTA}$* (*DTA*) sex-matched animals was monitored by high-resolution ultrasound (Vevo 2100 System, Visual Sonics) *in vivo*. Mice with mean tumor diameters > 5 mm were enrolled and treated with tamoxifen (+ TAM). Representative high-resolution ultrasound images from female mice pre-treatment (left, day 0) and after 7 d of TAM treatment (right panel) are shown. Visible lesions are outlined in white and tumor burden determined by automated three-dimensional (3D) B-mode imaging is shown in $mm^3$ in the lower right corner. Note: No tumors were detectable after 7 d of TAM treatment. (**e**) Representative macroscopic view of pancreata from tamoxifen-treated female *DTA* mice. (**f**) Representative H&E stains of tamoxifen-treated female *DTA* mice. (**g**) Female *Pdx1-Flp;FSF-R26$^{CAG\text{-}CreERT2}$;LSL-R26$^{DTA}$* (*DTA,* upper panel) and *Pdx1-Flp;FSF-R26$^{CAG\text{-}CreERT2/+}$* control (Ctrl, lower panel) animals were treated for 14 d with tamoxifen (+ TAM) and pancreata analyzed by H&E staining. (**h**) Serum lipase levels of *Pdx1-Flp;FSF-R26$^{CAG\text{-}CreERT2}$;LSL-R26$^{DTA}$* (*DTA*) and *Pdx1-Flp;FSF-R26$^{CAG\text{-}CreERT2/+}$* control (Ctrl) animals treated with tamoxifen (TAM). Scale bars, 50 µm.

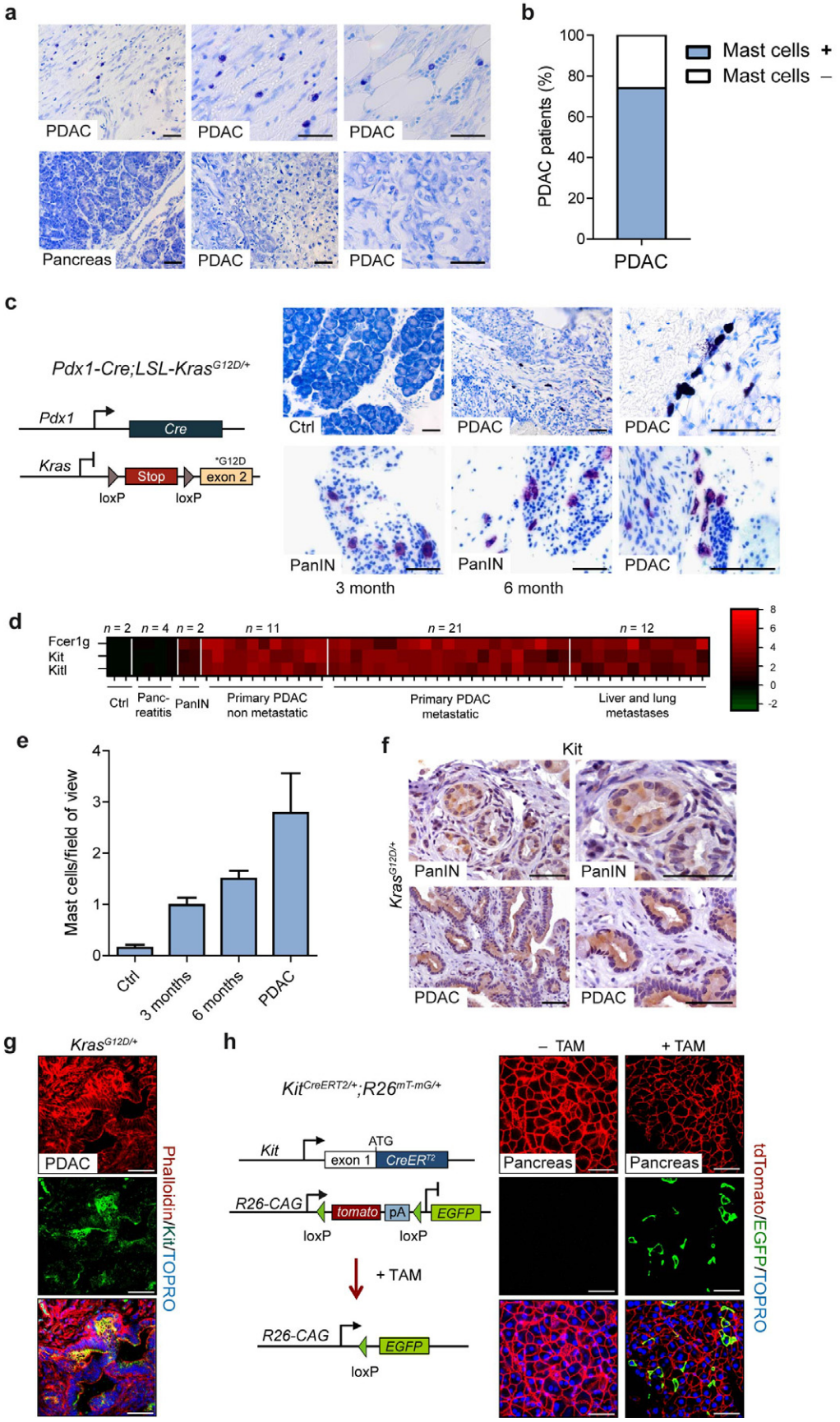


**Supplementary Figure 10** Mast cells infiltrate human and murine Kras-driven PDAC, but are dispensable for tumor initiation. (**a**) Human PDAC tissue microarrays (*n* = 96 PDAC samples) were analyzed by toluidine blue staining for metachromatic infiltrating mast cells (purple color).

Representative images of indicated human PDAC and normal pancreatic tissue sections with (upper panel) and without (lower panel) mast cell infiltration. (**b**) Bar graph shows the percentage of human PDAC samples with mast cell infiltration. (**c**) Genetic strategy to induce oncogenic Kras expression in the pancreas using the Cre/loxP recombination system (left panel). Representative images of toluidine blue stained metachromatic mast cells (purple color) of male and female WT control (Ctrl), and PanIN and PDAC bearing pancreata of *Pdx1-Cre;LSL-Kras*$^{G12D/+}$ mice (right panel). (**d**) qRT-PCR analysis of FcεRIg, c-Kit (Kit) and Kit ligand (Kitl) mRNA expression as surrogates of mast cell infiltration in pancreatic tissues of male and female mice with the indicated pathologies. Colors indicate fold change of mRNA expression vs. wild type control (Ctrl). (**e**) Quantification of infiltrating mast cells in male and female WT controls (Ctrl), and PanIN (3 and 6 months old) and PDAC bearing pancreata of sex-matched *Pdx1-Cre;LSL-Kras*$^{G12D/+}$ mice (mean, + s.e.m.; *n* = 3 of each genotype and time point; 20 fields of view per animal). (**f**) Representative immunohistochemical Kit staining of PanIN and PDAC from *Pdx1-Flp;FSF-Kras*$^{G12D/+}$ mice. (**g**) Immunofluorescence Kit staining (green color) of female *Pdx1-Flp;FSF-Kras*$^{G12D/+}$ induced PDAC. Cells were counterstained with phalloidin (red) and nuclei with TOPRO-3 (blue). (**h**) Kit lineage tracing strategy (left panel). Representative confocal microscopic images of tdTomato (red color, non Cre-recombined cells) and Cre-induced EGFP (green color) expression in the pancreas of tamoxifen (+ TAM) and vehicle (– TAM) treated *Kit*$^{CreERT2/+}$*;R26*$^{mT\text{-}mG/+}$ females (right panel). Note: CreER$^{T2}$ is expressed under the control of the endogenous *Kit* promoter enabling Kit lineage tracing *in vivo*. Scale bars, 50 µm.

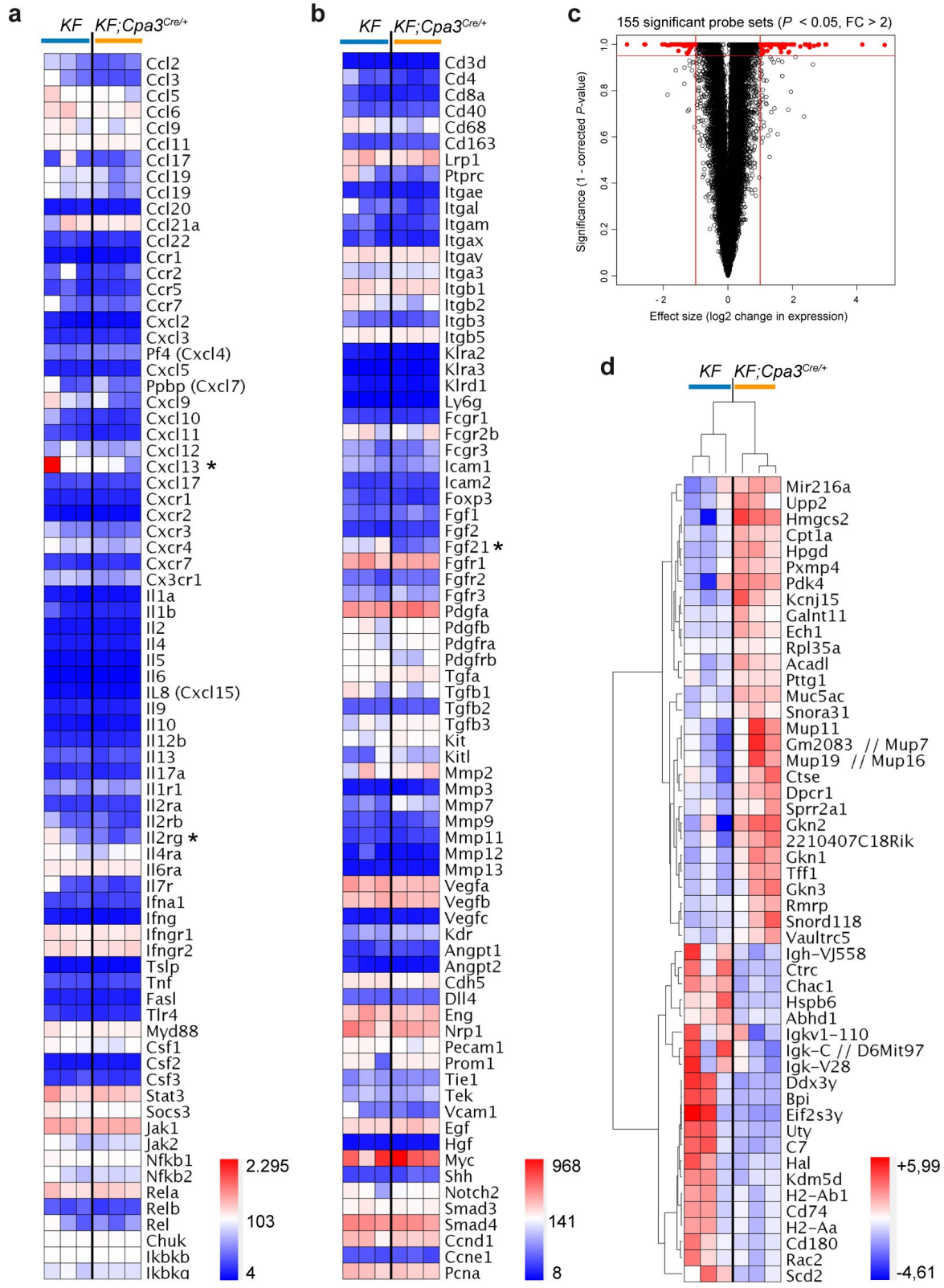


**Supplementary Figure 11** Gene expression changes in mast cell-deficient pancreatic tumors. Total RNA from pancreatic tumors of 12 month-old histologically verified mast cell-deficient *Pdx1-Flp;FSF-Kras$^{G12D/+}$;Cpa3$^{Cre/+}$* (*KF;Cpa3$^{Cre/+}$*) animals and controls with mast cell infiltration (*Pdx1-Flp;FSF-Kras$^{G12D/+}$; KF*) was analyzed by global gene expression arrays (*n* = 3 of each genotype).

(**a**) Selected cytokines, cytokine receptors and downstream targets with an established role in tumor biology are depicted in the heatmap. The genes listed were compared between *Pdx1-Flp;FSF-Kras*$^{G12D/+}$*;Cpa3*$^{Cre/+}$ animals and *Pdx1-Flp;FSF-Kras*$^{G12D/+}$ controls (*n* = 3 of each genotype). (**b**) The listed genes are markers for different cell types in the tumor microenvironment as well as growth factors and their cognate receptors, angiogenic factors, metalloproteinases, or signaling molecules previously implicated in pancreatic cancer biology. The heatmaps in (a) and (b) are globally normalized for all genes shown in each panel, and the color code (bottom right) shows the corresponding gene expression levels. Genes with significantly different mRNA expression changes >2 fold are marked by an asterisk in (a) and (b). (**c**) Volcano plot showing the comparison of global gene expression between the two investigated groups. Each circle corresponds to one probe set, the x-axis displays the log2 fold-change and the y-axis represents the corresponding multiple testing corrected *P*-value. 155 probe sets (red) corresponding to 108 annotated genes, showed significantly different >2 fold mRNA expression changes between both groups (*P*-value < 0.05, fold change > 2; cutoffs are shown as red lines). (**d**) Heatmap of the top 50 most significant > 2 fold differentially expressed genes shown in (c). Differentially expressed genes were filtered by standard deviation, subjected to statistical *t* tests, corrected for multiple testing, and hierarchically clustered by Pearson correlation. The color code (bottom right) shows the log2 fold-change in gene expression for each sample.

**Supplementary Table 1: Genotyping Primers**

| **Primer name** | **Sequence (5' - 3')** |
|---|---|
| Pdx1-Flp forward | AGAGAGAAAATTGAAACAAGTGCAGGT |
| Flp reverse | CGTTGTAAGGGATGATGGTGAACT |
| | |
| Kras Common forward | CACCAGCTTCGGCTTCCTATT |
| Kras WT reverse | AGCTAATGGCTCTCAAAGGAATGTA |
| Kras FSF MUT reverse | GCGAAGAGTTTGTCCTCAACC |
| | |
| hpAP forward | GAGAACCCGGACTTCTGGAAC |
| hpAP reverse | GTCTTGGACAGAGCCACATATG |
| | |
| R26 Common forward | AAAGTCGCTCTGAGTTGTTAT |
| hpAP Recombined reverse | CCTCCTCAACTGGGATGATGC |
| | |
| EGFP forward (*R26*$^{mT\text{-}mG}$ line) | TGCCCGAAGGCTACGTCCAG |
| EGFP reverse (*R26*$^{mT\text{-}mG}$ line) | CCATGTGATCGCGCTTCTCGT |
| | |
| R26 Common forward | AAAGTCGCTCTGAGTTGTTAT |
| R26 WT reverse | GGAGCGGGAGAAATGGATATG |
| R26$^{mT\text{-}mG}$ MUT reverse | GTACTTGGCATATGATACACTTGATGTAC |
| | |
| CreER$^{T2}$ forward (*R26*$^{CAG\text{-}CreERT2}$ line) | GAATGTGCCTGGCTAGAGATC |
| CreER$^{T2}$ reverse (*R26*$^{CAG\text{-}CreERT2}$ line) | GCAGATTCATCATGCGGA |
| | |
| R26 Common forward | AAAGTCGCTCTGAGTTGTTAT |
| R26 WT reverse | GGAGCGGGAGAAATGGATATG |
| R26$^{CAG\text{-}CreERT2}$ MUT reverse | TCAATGGGCGGGGGTCGTT |
| | |

| | |
|---|---|
| R26-CAG forward | GTTCGGCTTCTGGCGTGT |
| $CreER^{I2}$ recombined reverse | CGATCCCTGAACATGTCCATC |
| | |
| Gabra forward (Ctrl) | AACACACACTGGAGGACTGGCTAGG |
| Gabra reverse (Ctrl) | CAATGGTAGGCTCACTCTGGGAGATGATA |
| | |
| Pdk1 floxed forward | ATCCCAAGTTACTGAGTTGTGTTGGAAG |
| Pdk1 floxed reverse | TGTGGACAAACAGCAATGAACATACACGC |
| | |
| Pdk1 Recombined forward | CTATGCTGTGTTACTTCTTGGTGC |
| Pdk1 Non-Recombined forward | TCCCTCTAGCAAATGTTCTGTCT |
| Pdk1 common reverse | GGACAAACAGCAATGAACATACAC |

## SUPPLEMENTARY RESULTS

### Functional analysis of cell populations within the tumor microenvironment - Mast cells are dispensable for PDAC initiation

To demonstrate the utility of the DRS-based PDAC model as a means of targeting cells of the tumor microenvironment, we sought to clarify the role of mast cells in PDAC initiation. Previous studies had revealed apparently conflicting roles for mast cells in tumor biology. Many epidemiological studies reported that increased abundance of mast cells in the stroma of different tumor types is associated with a favorable prognosis[1-3]. Patients with high mast cell numbers showed increased survival rates and decreased risk of tumor recurrence after resection, and lower incidence of metastasis. However, some studies report that high numbers of tumor infiltrating mast cells are associated with poor patient outcome[4-7].

Results gained by combining murine tumor models with mast cell-deficient *Kit* mutant models (e.g. $Kit^{W\text{-}sh}$ mice) have also been conflicting. Some studies found an inverse correlation of mast cell abundance with tumor incidence and growth[8,9], while others reported pro-tumorigenic effects of mast cells, mainly attributed to increased angiogenesis[7,10-13]. By utilizing the novel DRS model, we show that mast cells are dispensable for PDAC initiation and progression, as evidenced by unaltered PanIN development and progression and PDAC formation in *Kit* independent mast cell deficient mice.

These findings can be reconciled because previous studies induced mast cell deficiency by *Kit* hypomorphism (e.g. $Kit^{W\text{-}sh}$ mice) or pharmacological inhibition of mast cell degranulation (disodium cromoglycate / cromolyn). Both strategies have major limitations; cromolyn may exert off-target effects and whole animal hypomorphism in Kit function may exert effects on cell types other than mast cells, because Kit signaling is implicated in the carcinogenesis of different tumor types. Indeed, we show that Kit is expressed in pancreas, PanIN lesions and PDAC. In addition, it is well known that $Kit^{W\text{-}sh/W\text{-}sh}$ animals suffer from severe defects in the hematopoietic system, which might alter tumor formation and progression. It is therefore essential to re-evaluate mast cell function in *Kit* independent models[14].

To gain insight into gene expression changes associated with mast cell deficiency, we performed global array-based mRNA expression profiling of pancreatic tumors from mast cell-deficient *Pdx1-Flp;FSF-Kras*$^{G12D/+}$*;Cpa3*$^{Cre/+}$ (KF,*Cpa3*$^{Cre/+}$) mice and *Pdx1-Flp;FSF-Kras*$^{G12D/+}$ (KF) control animals with mast cell infiltration (**Supplementary Fig. 11**). The presence and absence of mast cells in these tumors was histologically verified by toluidine blue staining. Although mast cells account for less than 0.5% of cells in pancreatic tumors of control animals, we obtained a statistically significant gene expression signature of mast cell deficiency in *Pdx1-Flp;FSF-Kras*$^{G12D/+}$*;Cpa3*$^{Cre/+}$ tumors using gene set enrichment analysis

(GSEA; Broad Institute, MIT), by comparing our gene expression data with mast cell deficient gene expression profiles[15] (Normalized Enrichment Score: -1.5837048 (negative enrichment/downregulation of mast cell gene sets); Nominal p-value: 0.008152174; False Discovery Rate (FDR) q-value: 0.0096 (< 1%); Familywise-Error Rate (FWER) *P*-Value: 0.024). Analysis for gene expression of chemokines and chemokine receptors, interleukins and interleukin receptors, chemoattractants, metalloproteinases, as well as Tnf, Ifng, Kit and Scf (Kitl), and of known cancer relevant growth factors and growth factor receptors, angiogenic factors, adhesion molecules, and intracellular signaling molecules and pathways previously implicated in PDAC formation[13,16-18], revealed no significant effects of mast cell ablation on these parameters, except for Cxcl13, Fgf21 and Il2rg (**Supplementary Fig. 11a,b** and data not shown). However, the effects on Cxcl13, Fgf21 and Il2rg were moderate and often not consistent within the respective group (e.g. Cxcl13; **Supplementary Fig. 11a**). Altogether, only 155 probe sets (0.44%) corresponding to 108 annotated genes, displayed significantly different >2 fold mRNA expression changes between both groups (**Supplementary Fig. 11c**). In addition to the aforementioned 3 genes, only cathepsin E (Ctse) and Muc5ac, which are significantly up-regulated in mast cell deficient tumors, have been linked to pancreatic disease (**Supplementary Fig. 11d**). These findings suggest that, in our system, cancer-relevant pathways are not broadly altered due to mast cell deficiency and corroborate our experimental observation that mast cells fail to influence PDAC development.

## REFERENCES


1. Nielsen, H.J.*, et al.* Independent prognostic value of eosinophil and mast cell infiltration in colorectal cancer tissue. *J Pathol* **189**, 487-495 (1999).
2. Rajput, A.B.*, et al.* Stromal mast cells in invasive breast cancer are a marker of favourable prognosis: a study of 4,444 cases. *Breast Cancer Res Treat* **107**, 249-257 (2008).
3. Tomita, M., Matsuzaki, Y. & Onitsuka, T. Correlation between mast cells and survival rates in patients with pulmonary adenocarcinoma. *Lung Cancer* **26**, 103-108 (1999).
4. Gulubova, M. & Vlaykova, T. Prognostic significance of mast cell number and microvascular density for the survival of patients with primary colorectal cancer. *J Gastroenterol Hepatol* (2007).
5. Chang, D.Z.*, et al.* Mast cells in tumor microenvironment promotes the in vivo growth of pancreatic ductal adenocarcinoma. *Clin Cancer Res* **17**, 7015-7023 (2011).
6. Strouch, M.J.*, et al.* Crosstalk between mast cells and pancreatic cancer cells contributes to pancreatic tumor progression. *Clin Cancer Res* **16**, 2257-2265 (2010).
7. Theoharides, T.C. Mast cells and pancreatic cancer. *N Engl J Med* **358**, 1860-1861 (2008).
8. Burtin, C.*, et al.* Inverse correlation between tumor incidence and tissue histamine levels in W/WV, WV/+, and +/+ mice. *J Natl Cancer Inst* **74**, 671-674 (1985).
9. Sinnamon, M.J.*, et al.* A protective role of mast cells in intestinal tumorigenesis. *Carcinogenesis* **29**, 880-886 (2008).

10. Wedemeyer, J. & Galli, S.J. Decreased susceptibility of mast cell-deficient Kit(W)/Kit(W-v) mice to the development of 1, 2-dimethylhydrazine-induced intestinal tumors. *Lab Invest* **85**, 388-396 (2005).
11. Coussens, L.M.*, et al.* Inflammatory mast cells up-regulate angiogenesis during squamous epithelial carcinogenesis. *Genes Dev* **13**, 1382-1397 (1999).
12. Soucek, L.*, et al.* Mast cells are required for angiogenesis and macroscopic expansion of Myc-induced pancreatic islet tumors. *Nat Med* **13**, 1211-1218 (2007).
13. Wöhrmann, S.M., Diakopoulos, K.N., Lesina, M. & Algül, H. The immune network in pancreatic cancer development and progression. *Oncogene* (2014).
14. Rodewald, H.-R. & Feyerabend, T.B. Widespread immunological functions of mast cells: fact or fiction? *Immunity* **37**, 13-24 (2012).
15. Feyerabend, T.B.*, et al.* Cre-mediated cell ablation contests mast cell contribution in models of antibody- and T cell-mediated autoimmunity. *Immunity* **35**, 832-844 (2011).
16. Pylayeva-Gupta, Y., Grabocka, E. & Bar-Sagi, D. RAS oncogenes: weaving a tumorigenic web. *Nat Rev Cancer* **11**, 761-774 (2011).
17. Morris, J.P.t., Wang, S.C. & Hebrok, M. KRAS, Hedgehog, Wnt and the twisted developmental biology of pancreatic ductal adenocarcinoma. *Nat Rev Cancer* **10**, 683-695 (2010).
18. Mazur, P.K. & Siveke, J.T. Genetically engineered mouse models of pancreatic cancer: unravelling tumour biology and progressing translational oncology. *Gut* **61**, 1488-1500 (2012).